Acta Oceanol. Sin., 2019, Vol. 38, No. 4, P. 136–145
https://doi.org/10.1007/s13131-018-1338-6
http://www.hyxb.org.cn
E-mail: hyxbe@263.net

Seasonal variability of the wind-generated near-inertial energy flux in the South China Sea

Baonan Sun[1, 2, 3], Zhan Lian[2, 3*], Yeli Yuan[1, 2, 3], Haiyang Xu[2]

[1] College of Oceanic and Atmospheric Sciences, Ocean University of China, Qingdao 266100, China

[2] Key Laboratory of Marine Science and Numerical Modeling, First Institute of Oceanography, Ministry of Natural Resources, Qingdao 266061, China

[3] Laboratory for Regional Oceanography and Numerical Modeling, Pilot National Laboratory for Marine Science and Technology (Qingdao), Qingdao 266237, China

Received 23 May 2018; accepted 5 July 2018

Abstract

After validated by the *in-situ* observation, the slab model is used to study the wind-generated near-inertial energy flux (NIEF) in the South China Sea (SCS) based on satellite-observed wind data, and its dependence on calculation methods and threshold criteria of the mixed layer depth (MLD) is investigated. Results illustrate that the total amount of NIEF in the SCS could be doubled if different threshold criteria of MLD are adopted. The NIEF calculated by the iteration and spectral solutions can lead to a discrepancy of 2.5 GW (1 GW=1×10^9 W). Results also indicate that the NIEF exhibits spatial and temporal variations, which are significant in the boreal autumn, and in the southern part of the SCS. Typhoons are an important generator of NIEF in the SCS, which could account for approximately 30% of the annual mean NIEF. In addition, deepening of the MLD due to strong winds could lead to a decrease of NIEF by approximately by 10%. We re-estimate the annual mean NIEF in the SCS, which is (10±4) GW and much larger than those reported in previous studies.

Key words: near-inertial energy flux, mixed layer depth, South China Sea, typhoon

Citation: Sun Baonan, Lian Zhan, Yuan Yeli, Xu Haiyang. 2019. Seasonal variability of the wind-generated near-inertial energy flux in the South China Sea. Acta Oceanologica Sinica, 38(4): 136–145, doi: 10.1007/s13131-018-1338-6

1 Introduction

The South China Sea (SCS) is one of the largest marginal seas of the West Pacific Ocean. Evidence indicates that turbulent mixing is remarkably higher in the SCS basin as compared to the open abyssal ocean (Klymak et al., 2011; Tian et al., 2009; Yang et al., 2015).

Active oceanic turbulent mixing would not be sustainable without external mechanical energy inputs (Huang, 1998). The wind-generated near-inertial energy flux (NIEF) would be able to propagate to the deep ocean and have the potential to contribute to abyssal mixing. Additionally, the NIEF can affect biogeochemistry and climate processes (Jochum et al., 2013). Therefore, estimating the NIEF in the SCS and investigating its variability is of importance to the energy balance, water mass features (Qu, 2000), ocean circulation (Yang et al., 2015), and biochemical characteristics in the area.

There are several observation- and numerical-model-dependent methods to estimate the NIEF (Alford, 2003; Alford et al., 2012; Silverthorne and Toole, 2009; Furuichi et al., 2008; Rimac et al., 2013; Zhai et al., 2009). Among them, the slab model proposed by Pollard and Millard (1970) is a simplified but effective method, which has been widely used in the investigation of wind-generated near-inertial motions (D'Asaro, 1985; Alford, 2001, 2003; Watanabe and Hibiya, 2002; Alford et al., 2012). Although results of the slab model in some cases are satisfactory, the global NIEF from the wind to the ocean estimated by the slab model still vary considerably (0.29–1.40 TW) due to various calculation methods and threshold criteria of mix layer depth (MLD). Therefore, it is necessary to investigate the effects of different calculation methods and threshold criteria of MLD on the NIEF, before the slab model is performed in real cases.

Studies of the NIEF in the SCS are relatively rare, and most of them were based on limited *in-situ* observational data (Chen et al., 2013; Liu et al., 2014; Sun et al., 2011). Yang et al. (2016) analyzed the relationship between the NIEF and oceanic vertical mixing in the SCS. Although the results are meaningful, the details could not be precisely depicted due to the coarse horizontal resolution (2°× 2°). Li et al. (2015) used the slab model to estimate the NIEF in the SCS, and obtained a total amount of approximately 4.4 GW (1 GW = 1×10^9 W). This work is insightful, but the results need further discussion. First, the MLD in Li et al. (2015) was defined as the depth where the temperature was 0.8°C less than the sea surface temperature (SST), which is disputed. There are several threshold criteria to determine the MLD, which can lead to significant differences in the MLD in the SCS (Jia et al., 2001; Sun et al., 2007). Therefore, it is necessary to investigate the

Foundation item: The National Natural Science Foundation of China under contract No. 40976016; the Basic Scientific Fund for the National Public Research Institutes of China under contract No. GY0217Q06; the National Science and Technology Major Project of the Ministry of Science and Technology of China under contract No. 2018YFF01014100; the Natural Science Foundation of Shandong Province, China under contract No. ZR2015PD009.

*Corresponding author, E-mail: lianzhan@fio.org.cn

impact of different criteria of the MLD on the NIEF. Second, the iteration method in the slab model used by Li et al. (2015) might underestimate the NIEF in some circumstances (Alford, 2003). Thus, it is vital to analyze the sensitivity of the NIEF in the SCS to calculation methods.

In addition to data and method, previous studies have shown that typhoons are particularly important to the total amount of NIEF (Alford et al., 2015a; D'Asaro et al., 2014). The SCS is often affected by typhoons. To date, most of NIEF studies were based on non-typhoon resolved numerical models or observations made under normal weather conditions. Therefore, quantifying the contribution of typhoons to the overall NIEF in the SCS is crucial to improve our understanding of this issue.

The aim of the work presented here is to estimate the NIEF estimation in the SCS, and investigate its dependence on the threshold criteria of the MLD and calculation methods of the slab model. It is important to note the difficulty in determining the precise amount of NIEF due to deficiencies in the available observation data. Therefore, estimating the reasonable range of the NIEF in the SCS and determining its sensitivity to certain factors is very meaningful.

The paper is organized as follows: Data and methods are described in Section 2. The spatiotemporal variation of the NIEF in the SCS using different calculation methods and threshold criteria of the MLD is examined in Section 3. Conclusions are presented in Section 4.

2 Data and methods

2.1 *Data*

We chose the quick scatterometer QSCAT/NCEP blended wind product (Milliff et al., 1999) and simple ocean data assimilation (SODA) reanalysis data (Carton et al., 2000) as inputs of the slab model. The spatiotemporal resolutions of these two datasets are 0.5°×0.5° per 6 h (QSCAT) and 0.5°×0.5°×40 vertical levels per month (SODA), respectively (the depth of vertical grids in the upper 300 m of SODA are 5, 15, 25, 35, 46, 57, 70, 82, 96, 112, 129, 148, 171, 197, 229 and 268 m). The temperature and salinity data from SODA were interpolated onto a 1 m vertical grid to calculate the MLD. Data from August 1999 to July 2009 were used in this study.

To validate QSCAT data and the slab model, a time series of *in-situ* ocean current data was used. The station was located at 19.939°N, 115.381°E (Fig. 1a), on the continental slope of the SCS. Current from 1 to 44 m depth with an interval of 1 m was measured by a down-looking ADCP, but the effective data range used in this study was approximately 5 to 35 m. Therefore, the vertical mean current within this range was regarded as the current in the

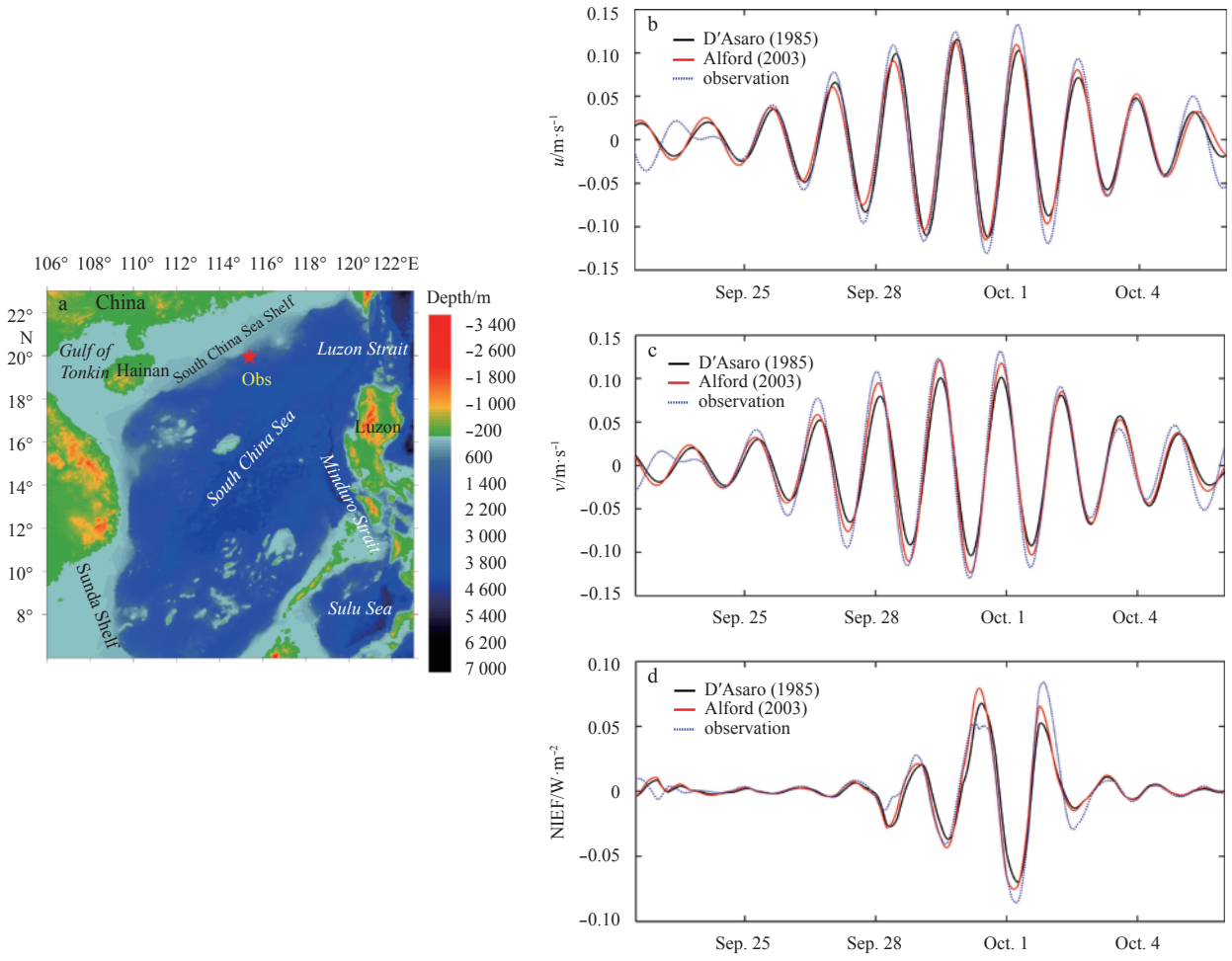

Fig. 1. The position of the station and the observational results. a. Bathymetry of the study area. The red star indicates the ADCP station. Observations were made from September 22 to October 6, 2007. b. Comparison of modeled (black and red lines) and observed (blue line) eastward near-inertial current. c. Same as b but for northward near-inertial current. d. Same as b but for the NIEF.

MLD. This *in-situ* observation was made from September 22 to October 6, 2007, within the operational period of the QSCAT satellite.

The best track data of typhoons used in this study were obtained from the Regional Specialized Meteorological Center.

2.2 *Methods*

Based on the QSCAT/NCEP wind stress product, we used the slab model to calculate the near-inertial current. The slab model was formulated as

$$\frac{\partial \boldsymbol{Z}}{\partial t}+(r+\mathrm{i}f)\boldsymbol{Z}=\frac{\boldsymbol{\tau}}{H}, \tag{1}$$

where $\boldsymbol{Z}$ is the complex current in the mixed layer, H is the MLD, f is the local inertial frequency, and r is the parameter presenting the decay of near-inertial motions. $\boldsymbol{Z}$ and $\boldsymbol{\tau}$ are expressed as

$$\boldsymbol{Z}=u+\mathrm{i}v, \tag{2}$$

$$\boldsymbol{\tau}=\frac{\tau_x+\mathrm{i}\tau_y}{\rho_\mathrm{w}}, \tag{3}$$

where u and v are the zonal and meridional current components in the mixed layer, τ_x and τ_y are the zonal and meridional components of wind stress respectively, and ρ_w is the density of sea water.

The definition of the mixed layer relies on different parameters. In this study, we compared three threshold criteria of MLD and investigate their effects on the calculated NIEF in the SCS:

Criterion 1: The depth where the temperature was 0.8°C less than that at 10 m below the sea surface ($T_{10\,\mathrm{m}}$; Kara et al., 2000).

Criterion 2: The depth where the density was equal to the density at 0.5°C less than $T_{10\,\mathrm{m}}$ (Sprintall and Tomczak, 1992).

Criterion 3: The depth where the temperature was 0.2°C less than $T_{10\,\mathrm{m}}$ or density was 0.03 kg/m^3 greater than $\rho_{10\,\mathrm{m}}$ (the density of sea water at 10 m below the sea surface), according to De Boyer Montégut et al. (2004).

In this study, the reference depth of MLD was 10 m. This depth was selected because the SCS is located in the tropics and experiences a high frequency of rainfall when wind speed is low and vertical mixing is weak. Consequently, a "fresh lid" often emerges in the surface layer of the SCS. The disturbance induced by this abnormal "fresh lid" can be avoided at 10 m (Sprintall and Roemmich, 1999). Regions with water depth shallower than 10 m were not considered.

There are two methods to solve $\boldsymbol{Z}$ in Eq. (1). The first method was proposed by D'Asaro (1985), which is renamed as "interation solution" in this study for convenience. For a known initial value $\boldsymbol{Z}_{t_1}$, at any given moment t_2, $\boldsymbol{Z}_{t_2}$ can be calculated as

$$\boldsymbol{Z}_{t_2}=\boldsymbol{Z}_{t_1}\mathrm{e}^{-\omega\Delta t}-\frac{\Delta\boldsymbol{\tau}/\Delta t}{H\omega^2}(1-\mathrm{e}^{-\omega\Delta t}), \tag{4}$$

where $\Delta t=t_2-t_1$, $\Delta\boldsymbol{\tau}$ is the change of $\boldsymbol{\tau}$ over the interval Δt, $\omega = r+\mathrm{i}f$, and r is 0.15f. Li et al. (2015) estimated the NIEF in the SCS by this method. However, according to Alford (2003), this method could underestimate the total flux under certain circumstances. Therefore, the improved "spectral solution" was proposed by Alford (2003). In this method, r in Eq. (1) is set as a variable depending on frequency (σ). It is expressed as $r(\sigma)=r_0(1-\mathrm{e}^{-\sigma^2/2\sigma_c^2})$, where $r_0=0.15f$ and decays to zero for $\sigma<\sigma_c\equiv f/2$. To solve Eq. (1) in the frequency domain, a transfer function was implemented, $R=\tilde{\boldsymbol{Z}}(\sigma)/\tilde{\boldsymbol{\tau}}(\sigma)$, linking the spectrum of the mixed-layer current to that of $\boldsymbol{\tau}$ (where $\tilde{\boldsymbol{Z}}(\sigma)$ and $\tilde{\boldsymbol{\tau}}(\sigma)$ denote the Fourier transforms of $\boldsymbol{Z}$ and $\boldsymbol{\tau}$ at frequency σ). To Eq.(1),

$$R(\sigma)=\frac{1}{H}\frac{r-\mathrm{i}(f+\sigma)}{r^2+(f+\sigma)^2}. \tag{5}$$

For every grid, Fourier transformation was first performed to the wind stress time series to obtain $\tilde{\boldsymbol{\tau}}(\sigma)$. The transfer function (5) was then applied to calculating $\tilde{\boldsymbol{Z}}(\sigma)=R(\sigma)\tilde{\boldsymbol{\tau}}(\sigma)$. Through inverse Fourier transformation, $\boldsymbol{Z}$ could be finally obtained. In this study, we compared the iteration and spectral solutions of Eq. (1).

Given that MLD typically changes more slowly than wind-stress fluctuations, in Eqs (4) and (5), $H=H_\mathrm{ref}=50$ m, according to Alford (2001). The NIEF with the reference MLD ($\Pi(H_\mathrm{ref})$) was computed as

$$\Pi(H_\mathrm{ref})=Re(\rho_\mathrm{w}\boldsymbol{Z}\boldsymbol{\tau}^*). \tag{6}$$

Using six-hourly wind-stress time series, iteration and spectral solutions were calculated at each grid in the SCS. This enabled computation of the flux in "typical" mixed layer conditions from a time series of wind stress alone. By determining the MLD at a given location and time, the actual NIEF ($\Pi(H)$) can be computed as follows:

$$\Pi(H)=\frac{H_\mathrm{ref}}{H}\Pi(H_\mathrm{ref}). \tag{7}$$

To examine the sensitivity of NIEF to typhoons, we eliminated the effect of typhoons using the following method. The influential region of a typhoon was defined as a circle, of which the center is that of the typhoon and the radius is that of 30 kn (1 kn ≈ 0.51 m/s) wind speeds. Both typhoon centers and radii of 30 kn wind speeds were obtained from the best track data. Wind stress data within the influential region of typhoons were replaced by the interpolated results of wind stress on the grids outside the influential region. Under the influence of typhoons, the MLD may increase due to the strong surface forcing (Li and Wen, 2017). In this study, this response was parameterized by setting it as a function of the distance from the typhoon track and the time after typhoon occurrence according to the statistical results of Wu and Chen (2012). Under this approximation, the characteristic period for MLD variations was approximately 5 d, which was still much longer than the corresponding values of wind stress data (6 h). Therefore, the assumption that the differential term of MLD with respect to time is much smaller than that of wind stress still holds true

3 Results and discussion

3.1 *Verification of slab model result based on in-situ observations*

The near-inertial currents driven by QSCAT/NCEP wind stress through the methods of D'Asaro (1985) and Alford (2003) were compared with mooring observations (applying a band-pass filter of 0.85f–0.15f) and shown in Figs 1b and c. In the slab model, the MLD at the mooring was set as a constant (35 m). The vertical averaged (5–35 m) current from observations was regarded as the current in the mixed-layer and compared with the

simulated results of the slab model. As seen from Figs 1b and c, both iteration and spectral solutions of the slab model are comparable to the observations. Similar pattern could be also seen from the NIEF shown in Fig. 1d, although Plueddemann and Farrar (2006) suggested that the slab model, despite accurately reproducing the amplitude and phase of the velocity response, often overestimated work because of its neglect of dissipative processes at the base of the mixed layer. However, it should be noted that the peaks of the spectral solution were closer to observations than those of the iteration solution. The root mean square errors (RMSE) between modeled and observed vertical mean currents were 0.015 m/s (eastward, iteration solution), 0.011 m/s (eastward, spectral solution), 0.019 m/s (northward, iteration solution), and 0.011 m/s (northward, spectral solution). The RMSE of the NIEF was 0.010 W/m^2 for iteration solution and 0.008 W/m^2 for spectral solution. The spectral solution reduced the RMSE by 20%, which may be considered as quantitative proof indicating the superiority of the spectral solution.

These results indicate that (1) the QSCAT/NCEP wind stress product is suitable for studying the NIEF in the SCS; (2) both the iteration and spectral solutions could represent the basic traits of the NIEF; (3) the spectral solution is more accurate than the iteration solution, especially for large near-inertial currents.

3.2 *Sensitivity of NIEF to MLD threshold criteria and calculation methods*

In this section, the sensitivity of NIEF to different MLD threshold criteria and calculation methods was investigated. Four experiments with different combinations of MLD threshold criteria and calculation methods were considered, of which for the details are shown in Table 1. In M1–M3, the iteration solution of Eq. (1) was calculated with the three MLD threshold criteria introduced in Section 2.2, respectively. In M4, the spectral solution was calculated with the same MLD threshold criterion as in M3.

Table 1. Design of the four experiments

	MLD threshold criterion	Solution of equations
M1	Kara et al. (2000)	D'Asaro (1985)
M2	Sprintall and Tomczak (1992)	D'Asaro (1985)
M3	De Boyer Montégut et al. (2004)	D'Asaro (1985)
M4	De Boyer Montégut et al. (2004)	Alford (2003)

3.2.1 *MLD calculated from different threshold criteria*

The spatial patterns of MLD in the SCS in M1–M3 are presented in Fig. 2. In the boreal winter, smaller MLD mainly appeared to the west of the Luzon Island and larger MLD to the south of the Luzon Island. In the boreal summer, the isobaths of MLD were basically along the northeast-southwest direction, and the MLD to the northwest was smaller than that to the southwest. While the overall spatial pattern was consistent, the horizontal gradient and mean value of MLD differed markedly and gradually decreased from M1 to M3. The spatial mean MLD in the SCS without the shading area shown in Fig. 2 are calculated and listed in Table 2. The result suggests that the difference resulting from different threshold criteria was more remarkable in boreal winter than that in summer.

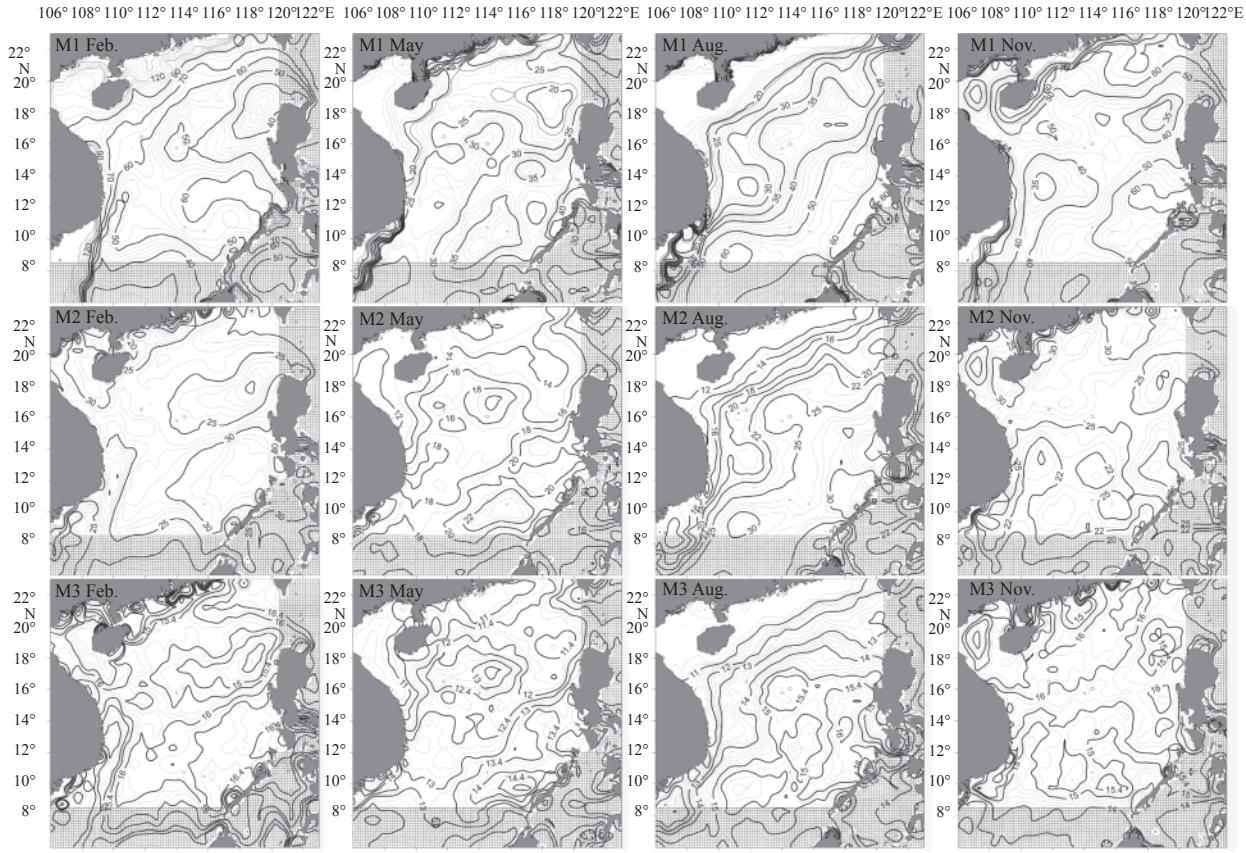

Fig. 2. Spatial pattern of monthly mean MLD (m) in February, May, August and November (horizontal sets) calculated from different threshold criteria (vertical sets). Note that the spatial mean MLD was calculated in the SCS without the shading area.

Table 2. Spatial mean MLD in M1–M3

	Spatial mean of MLD/m			
	Feb.	May	Aug.	Nov.
M1	69.81	28.87	36.69	54.56
M2	27.52	16.66	20.72	25.86
M3	15.81	12.31	13.48	15.63
Standard deviation	28.41	8.59	11.88	20.18

3.2.2 *NIEF obtained by different calculation methods with different MLD threshold criteria*

Figure 3 displays the spatial pattern of NIEF in February, May, August, and November in M1–M4. On the whole, the spatial pattern of NIEF in M1–M4 was similar in the SCS while the magnitude of NIEF exhibited significant difference. In February, the NIEF in the SCS was small except the northwest of Luzon Island and southwest of the Indo-China Peninsula. Large NIEF moved to the west of Luzon Island and the SCS shelf during May and August. In November, almost the entire SCS basin had large NIEF. This spatial pattern is similar to the results of Li et al. (2015; the same as M1 in this study, which gave the smallest NIEF among M1–M4).

The seasonal variability of NIEF in the SCS (larger in summer and smaller in winter) is contrary to the fact that wind stress is more intense in winter than summer (Lian et al., 2015). In order to explore the possible cause, we applied a band-pass filter, the same as described in Section 3.1, to the wind stress data, and calculated the standard deviation of the filtered data (Fig. 4). A larger standard deviation suggests that near-inertial band variation is more significant. This result indicates that the near-inertial band variations of wind stress (NIWS) are more robust in summer than winter and the positions with large NIWS and NIEF are co-located. This result further validates the accuracy fidelity of the slab model.

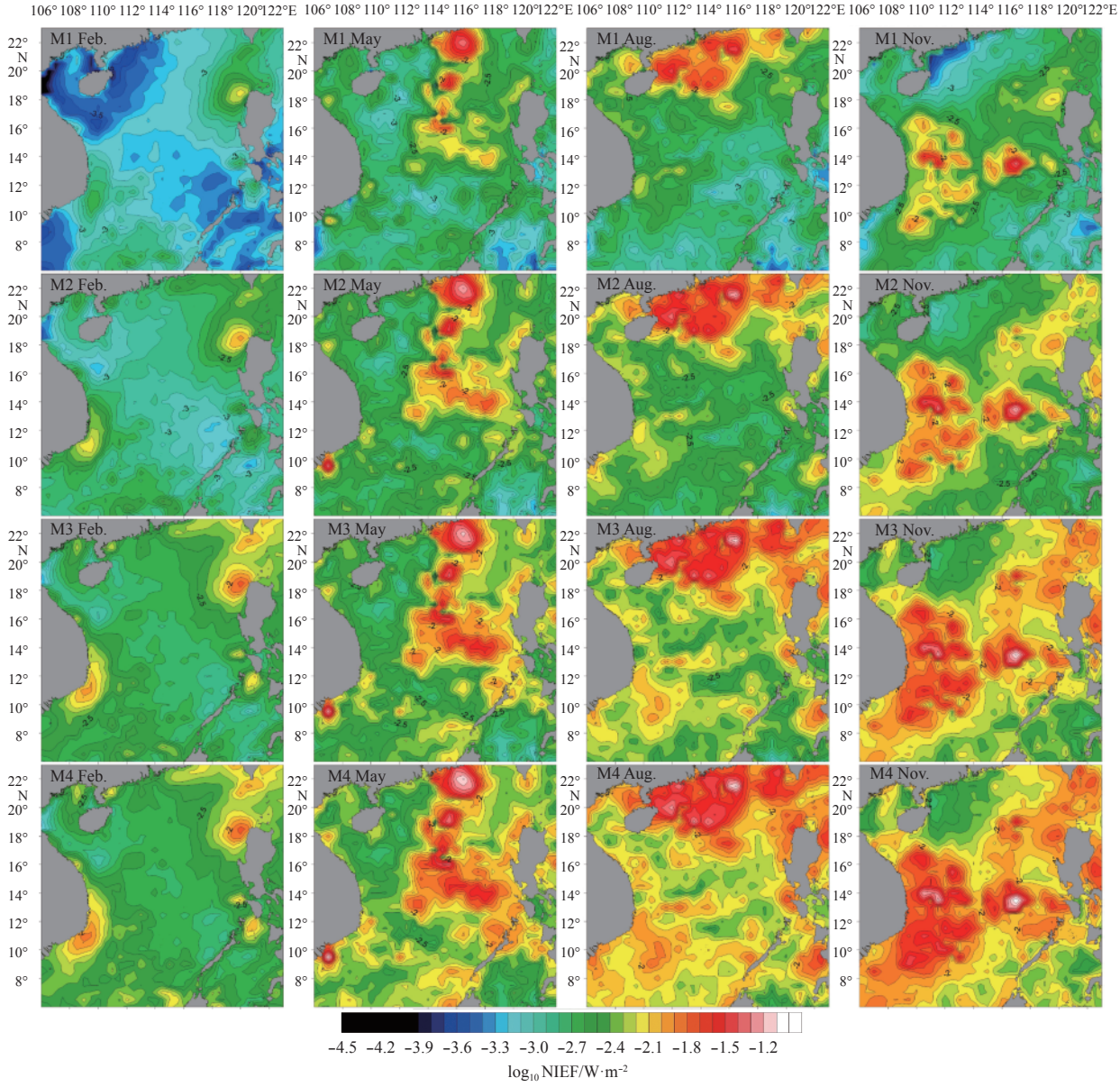

Fig. 3. Spatial pattern of monthly mean NIEF (in the form of $\log_{10}$) in February, May, August and November (horizontal sets) in the four cases (vertical sets).

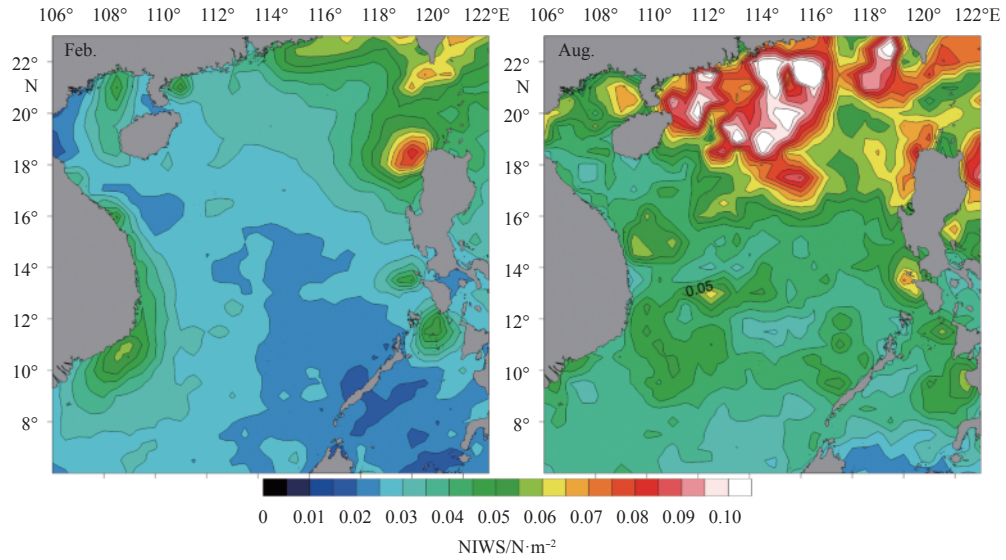

Fig. 4. The near-inertial band variations of wind stress in February (a) and August (b).

The spatial mean NIEF in M1–M4 was calculated to investigate its seasonal variation. At the same time, the SCS was divided into four areas (A1–A4, Fig. 5a), and the mean NIEF therein was calculated, respectively. The climatology monthly mean NIEF, as well as its standard deviations in each area and the entire SCS in M1–M4 are shown in Figs 5b–f. As seen, the maximum NIEF in areas A1–A4 appeared at different months, which are September in A1 and A2, and November in A3 and A4. Correspondingly, larger standard deviation appeared accompanied with larger NIEF. The largest absolute standard deviation was emerged in September in A1, and the second largest was in November in A3. In general, the differences between methods were smaller during the first half of the calendar year, except in A4.

It is important to note that, although obvious difference existed for the MLD in boreal winter due to different threshold criteria, there was no apparent difference in the NIEF. Instead, the standard deviation in February was significantly smaller than those in other months. This suggests that the difference of spatial mean NIEF was out of phase with the MLD.

For ocean mixing, researchers generally focus on the total amount of NIEF. By integrating the spatial monthly mean NIEF in the SCS, we estimated the total amount of NIEF in different areas (Table 3). The total NIEF in the entire SCS varied from 5.67 GW to 15.92 GW with the maximum value almost three times larger than the minimum. For different MLD threshold criteria, it is found that the total NIEF in the entire SCS in M2 and M3 was about 1.7 and 2.4 times larger than that in M1 respectively, suggesting that the model is sensitive to the MLD threshold criteria. At the same time, we found that the NIEF in M1–M3 was smaller than that in M4, indicating that the iteration solution indeed un-

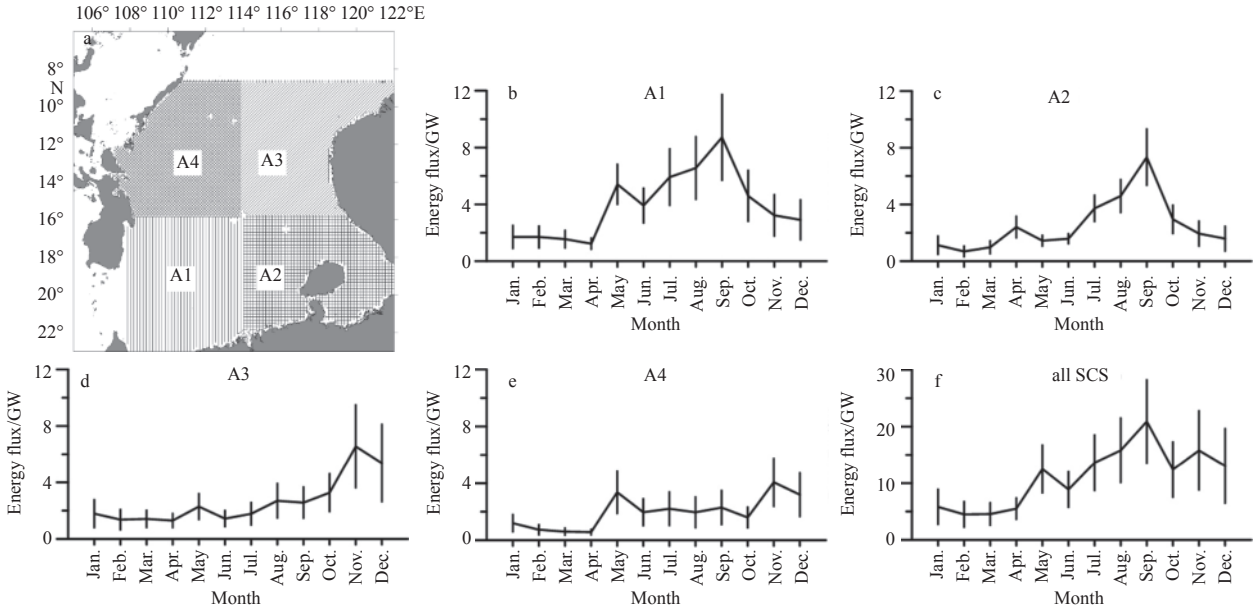

Fig. 5. A sketch of area division of the SCS (a), and the climatological monthly mean NIEF (polylines) and its standard deviations (vertical bars) in A1 (b), A2 (c), A3 (d), A4 (e) and the entire SCS (f).

Table 3. Total NIEF and its relative standard deviation in different areas and in the entire SCS

	M1/GW	M2/GW	M3/GW	M4/GW	Relative standard deviation
A1	2.14	3.48	4.78	5.41	0.36
A2	1.48	2.25	2.95	3.43	0.33
A3	1.19	2.18	3.19	4.04	0.47
A4	0.86	1.55	2.46	3.04	0.49
Entire SCS	5.67	9.48	13.38	15.92	0.40

derestimate the NIEF when compared with the spectral solution.

We also calculated the relative standard deviation of NIEF in different areas, which reached the largest in Area A4 where the total NIEF was the smallest. In addition, comparing the relative standard deviation in the four areas, it can be deduced that the southern part of the SCS (Areas A3 and A4) is more sensitive to MLD threshold criteria than the northern part (Areas A1 and A2).

As shown in Table 3, the total NIEF in the entire SCS in M1 (5.67 GW) is a little larger than that (4.4 GW) in Li et al. (2015), although the same method was used. There are two possible causes. The one is that Li et al. (2015) neglected the NIEF in areas with water depth shallower than 75 m, while the value is 10 m in this study. The other is that we interpolated the temperature and salinity from SODA onto 1 m vertical grids before calculating the MLD, while Li et al. (2015) used the original SODA data to determine the MLD.

3.3 *Effect of typhoons*

To study the effect of typhoons on the NIEF and estimate the proportion of NIEF induced by typhoons in the SCS, we discarded wind stress data within the influential range of typhoons, and then calculated the NIEF (hereafter referred as the no-typhoon case). The results from M1 to M4 in the no-typhoon case are presented in Fig. 6. We found that the spatial pattern of NIEF

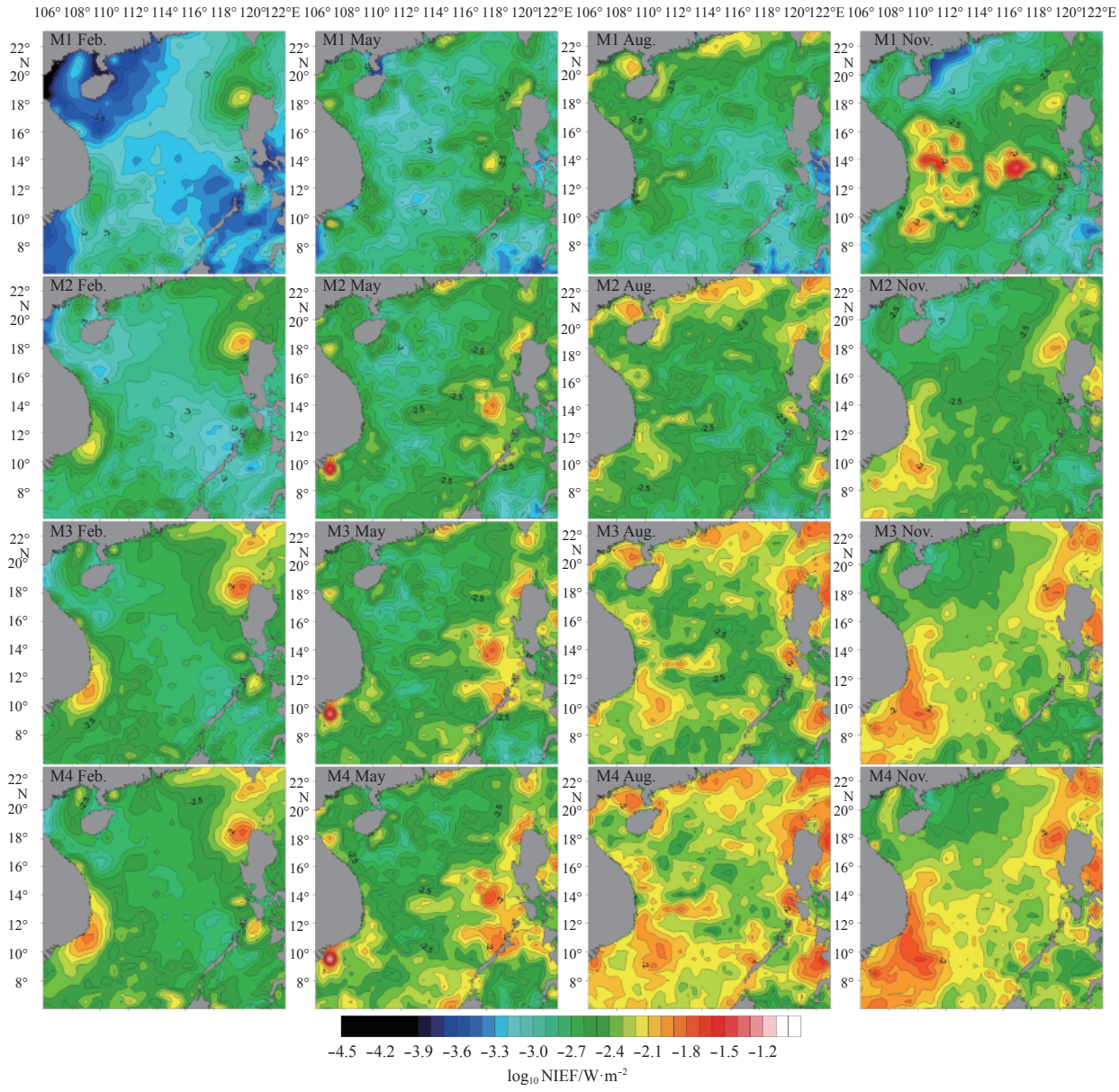

Fig. 6. Spatial pattern of monthly mean NIEF (in the form of $\log_{10}$) in February, May, August and November (horizontal sets) in the four no-typhoon cases (vertical sets).

in the no-typhoon case was significantly different from that using the original wind stress data (shown in Fig. 3 and hereafter referred as the original case), especially in May, August and November. In May, large NIEF in the northeast SCS basin disappeared, while that along the edge of the SCS basin varied slightly. The most remarkably large NIEF occurred near the Mindoro Strait. This spatial pattern continued into August, during which it was even more distinct. The change of NIEF in the southern part of the SCS was smaller than that in the northern part, indicating that the NIEF in this area was less affected by typhoons. In November, the NIEF showed a similar to that in February. Areas with large differences in the NIEF between the two cases shifted to the southeast coast of the Indo-China Peninsula.

We also calculated the climatological monthly mean NIEF and its standard deviations (Fig. 7) in the no-typhoon case. The results confirm that typhoons were a generator of NIEF in the SCS, particularly after April. The annual mean NIEF was 7.43 GW in the no-typhoon case, while it was 11.01 GW in the original case (the value averaged among M1–M4). In other words, typhoons contributed to almost 33% of the total NIEF in the SCS. Note that the contribution of typhoons in the total NIEF is not homogeneous in the SCS. The NIEF in Areas A1–A4 was 2.3, 1.5, 2.0 and 1.5 GW in the no-typhoon case, while it was 3.9, 2.5, 2.7 and 1.9 GW in the original case, suggesting that the contributions of typhoons in the total NIEF were 41%, 40%, 26% and 21% in the four areas, respectively. This means that typhoons are more important for NIEF in the northern part of SCS than in the southern part. The relative standard deviation increased slightly from 0.40 for the original case to 0.42 for the no-typhoon case. This result suggests that the sensitivity of the NIEF to the calculation methods was not significantly affected by typhoons.

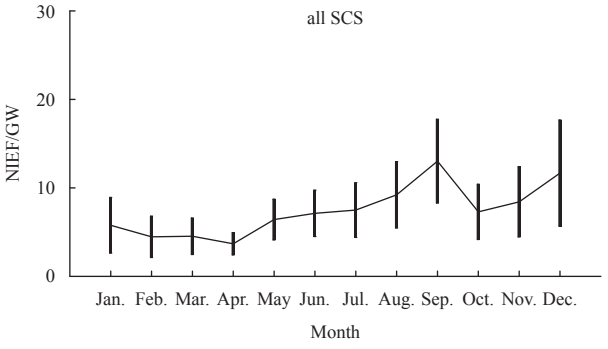

Fig. 7. The climatological monthly mean NIEF (polylines) and its standard deviations (vertical bars) in the SCS for the no-typhoon case.

As reported in other studies, during strong wind events (e.g., typhoons), the MLD can be increased by stirring from surface wind stress (D'Asaro et al., 2014; Pan and Sun, 2013; Wu and Chen, 2012). In the present slab model, the MLD and surface wind stress are decoupled. Therefore, the quantification of changes in the NIEF due to the deepened MLD induced by the typhoons is meaningful. The results obtained by considering the deepening of MLD induced by typhoons are presented in Fig. 8 (hereafter referred as the new MLD case). In this case, the magnitude of NIEF was smaller than that in the original case. The NIEF almost decreased by a factor of about 10% (9.95 GW) with a relative standard deviation of 0.41. Comparing results shown in Figs 5f and 9, it is found that the decrease of NIEF in the new MLD case mainly occurred after April. In addition, the contribution of typhoons in the total NIEF was 25% in the new MLD case.

4 Conclusions

As verified by the *in-situ* observation, we confirmed that the current calculated from the slab model and QSCAT wind product is suitable for the study of NIEF in the SCS. This comparison also presented a quantitative proof to demonstrate the superiority of the spectral solution of slab model.

Through analyses, we found that the NIEF in the SCS is fairly sensitive to the calculation method and the MLD threshold criterion. For different MLD threshold criteria, the maximum NIEF could be almost two times larger than the minimum value. Given that the SCS lies at low latitudes with frequent rainfall and a thin unstable layer of low temperature in the upper ocean, a threshold criterion considering both temperature and salinity is more reasonable (Sun et al., 2007). Based on the comparison between *in-situ* observations and simulated results of the slab model, it is suggestted that M4 is more appropriate in this study. This result suggests that Li et al. (2015; 4.4 GW) might underestimate the total NIEF in the SCS. By contrast, we suggest that the total flux should be around (10±4) GW.

Results also indicate that the NIEF exhibits spatial and temporal variations, which are significant in the boreal autumn and in the southern part of the SCS. The reason may be the combination of stronger NIWS and the more remarkable diversity of MLD. Because of the multiplying algebraic expression (as seen from Eq. (7)), the latter could be amplified by the former during this time. The different stratification of the upper ocean could be attributed to the diversity of MLD. During the active period of NIEF, the MLD in the southern SCS is deeper than the northern part, which could enhance the discrepancy among results from different MLD criterions. It might be the potential reason for the larger relative difference.

Through diagnostic analysis, we conclude that typhoons contribute to approximately 30% (33% compared with the original case, 25% compared with the new MLD case) of the annual mean NIEF in the SCS. Typhoons, as well as the variations in MLD induced by them do not significantly affect the sensitivity of the NIEF to the calculation method.

Considering the decay of near-inertial motion and excluding the energy lost within the upper layer (about 70% according to Von Storch et al. (2007)), there was about (3±1) GW of energy that could contribute to abyssal mixing. This value is considerable when compared to the tidal energy flux from Luzon Strait into the SCS (4–5 GW) (Alford et al., 2015b; Jan et al., 2008; Tian et al., 2009). It further confirms that near-inertial energy induced by wind is one of the most important energy sources for sustaining abyssal mixing in the SCS.

Convection caused by surface cooling is an important factor influencing the winter MLD in the SCS and further affecting the NIEF, and this effect should be considered in following studies. Furthermore, there are some other sources of uncertainty which have not been considered in this paper, such as the temperature thresholds in the criteria (0.8°C, 0.5°C and so on). Therefore, more long-term *in-situ* ocean observation data are required to more accurately verify the estimated results in the future.

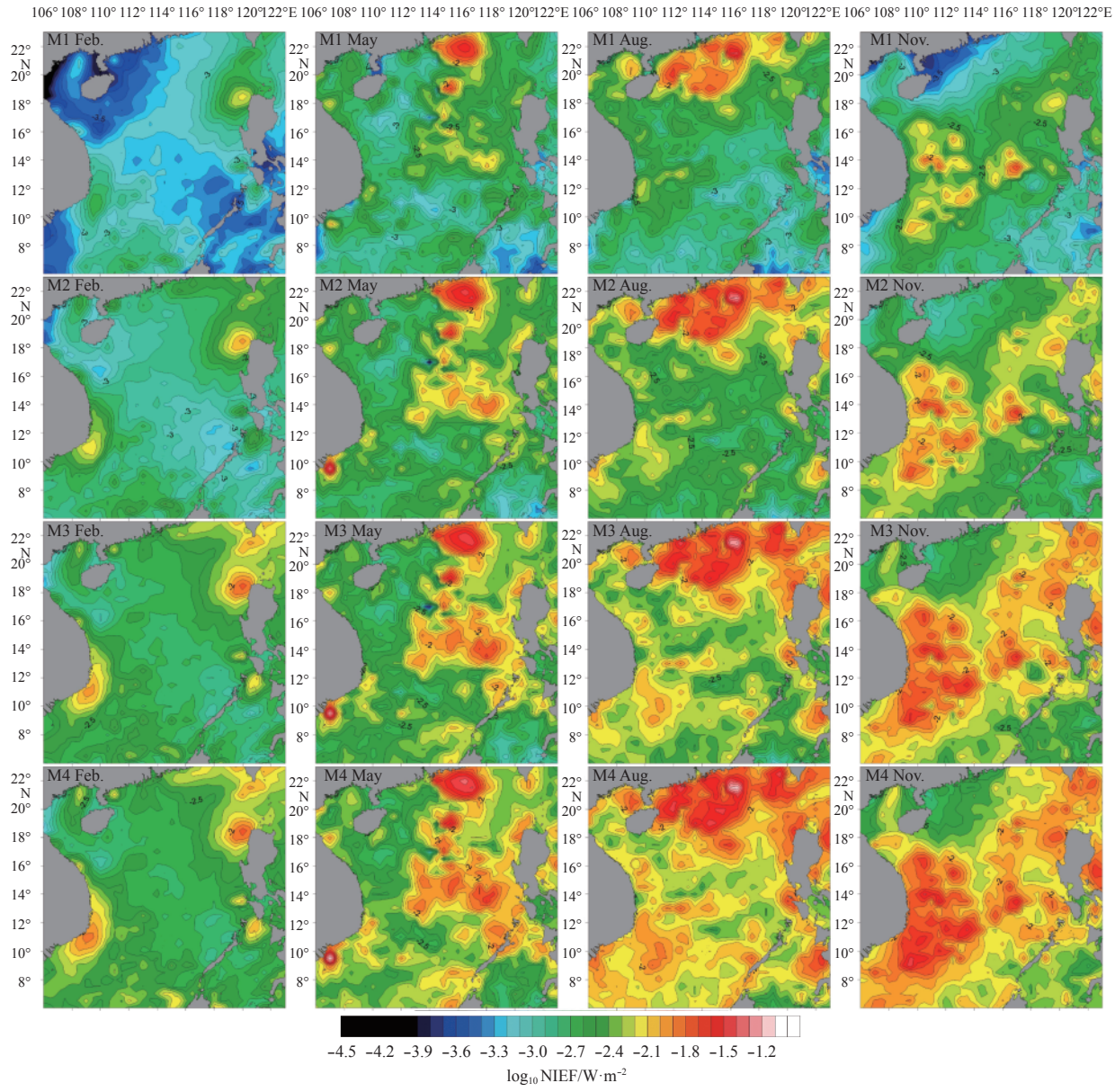

Fig. 8. Spatial pattern of monthly mean NIEF (in the form of $\log_{10}$) in February, May, August and November (horizontal sets) in the four new MLD cases (vertical sets).

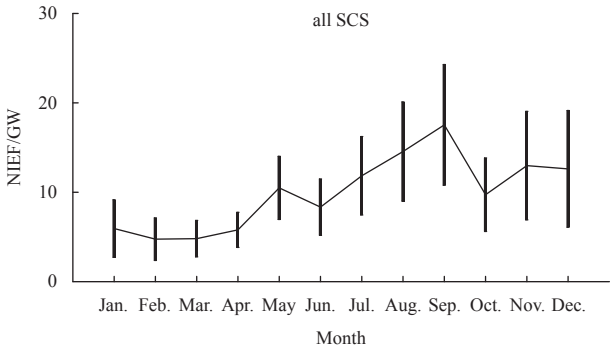

Fig. 9. The climatological monthly mean NIEF (polylines) and its standard deviations (vertical bars) in the SCS for the new MLD case.

Acknowledgements

Acknowledgement for the mooring data support from "National Earth System Science Data Sharing Infrastructure, National Science & Technology Infrastructure of China (http://www.geodata.cn)"; QSCAT/NCEP blended ocean winds are managed by the Data Support Section of the Computational and Information Systems Laboratory at the National Center for Atmospheric Research in Boulder, Colorado (http://rda.ucar.edu/datasets/ds744.4/); SODA data were provided by the SODA/TAMU research group, Texas A&M University (http://soda.tamu.edu/); the best track typhoon data sets were available at http://www.jma.go.jp/jma/jma-eng/jma-center/rsmc-hp-pub-eg/besttrack.html.

References

Alford M H. 2001. Internal swell generation: the spatial distribution of energy flux from the wind to mixed layer near-inertial motions. Journal of Physical Oceanography, 31(8): 2359–2368, doi:

10.1175/1520-0485(2001)031<2359:ISGTSD>2.0.CO;2
Alford M H. 2003. Improved global maps and 54-year history of wind-work on ocean inertial motions. Geophysical Research Letters, 30(8): 1424–1429
Alford M H, Cronin M F, Klymak J M. 2012. Annual cycle and depth penetration of wind-generated near-inertial internal waves at ocean station papa in the northeast Pacific. Journal of Physical Oceanography, 42(6): 889–909, doi: 10.1175/JPO-D-11-092.1
Alford M H, Mackinnon J A, Simmons H L, et al. 2015a. Near-inertial internal gravity waves in the ocean. Annual Review of Marine Science, 8: 95–123
Alford M H, Peacock T, Mackinnon J A, et al. 2015b. The formation and fate of internal waves in the South China Sea. Nature, 528(7580): 65–69
Carton J A, Chepurin G, Cao Xianhe, et al. 2000. A simple ocean data assimilation analysis of the global upper ocean 1950-95. Part I: methodology. Journal of Physical Oceanography, 30(2): 311–326, doi: 10.1175/1520-0485(2000)030<0311:ASODAA>2.0.CO;2
Chen Gengxin, Xue Huijie, Wang Dongxiao, et al. 2013. Observed near-inertial kinetic energy in the northwestern South China Sea. Journal of Geophysical Research: Oceans, 118(10): 4965–4977, doi: 10.1002/jgrc.20371
D'Asaro E A. 1985. The energy flux from the wind to near-inertial motions in the surface mixed layer. Journal of Physical Oceanography, 15(8): 1043–1059, doi: 10.1175/1520-0485(1985)015<1043:TEFFTW>2.0.CO;2
D'Asaro E A, Black P G, Centurioni L R, et al. 2014. Impact of typhoons on the ocean in the Pacific. Bulletin of the American Meteorological Society, 95(9): 1405–1418, doi: 10.1175/BAMS-D-12-00104.1
De Boyer Montégut C, Madec G, Fischer A S, et al. 2004. Mixed layer depth over the global ocean: An examination of profile data and a profile-based climatology. Journal of Geophysical Research: Oceans, 109(C12): C12003, doi: 10.1029/2004JC002378
Furuichi N, Hibiya T, Niwa Y. 2008. Model-predicted distribution of wind-induced internal wave energy in the world's oceans. Journal of Geophysical Research: Oceans, 113(C9): C09034
Huang Ruixin. 1998. Mixing and available potential energy in a boussinesq ocean. Journal of Physical Oceanography, 28(4): 669–678, doi: 10.1175/1520-0485(1998)028<0669:MAAPEI>2.0.CO;2
Jan S, Lien R C, Ting C H. 2008. Numerical study of baroclinic tides in Luzon Strait. Journal of Oceanography, 64(5): 789–802, doi: 10.1007/s10872-008-0066-5
Jia Xujing, Liu Qinyu, Sun Jilin. 2001. A comparison between two different definitions of the mixlayer and the thermocline in the South China Sea. Transactions of Oceanology and limnology, (1): 1–7
Jochum M, Briegleb B P, Danabasoglu G, et al. 2013. The impact of oceanic near-inertial waves on climate. Journal of Climate, 26(9): 2833–2844, doi: 10.1175/JCLI-D-12-00181.1
Kara A B, Rochford P A, Hurlburt H E. 2000. An optimal definition for ocean mixed layer depth. Journal of Geophysical Research: Oceans, 105(C7): 16803–16821, doi: 10.1029/2000JC900072
Klymak J M, Alford M H, Pinkel R, et al. 2011. The breaking and scattering of the internal tide on a continental slope. Journal of Physical Oceanography, 41(5): 926–945, doi: 10.1175/2010JPO4500.1
Li Juan, Liu Junliang, Cai Shuqun, et al. 2015. The spatiotemporal variation of the wind-induced near-inertial energy flux in the mixed layer of the South China Sea. Acta Oceanologica Sinica, 34(1): 66–72, doi: 10.1007/s13131-015-0597-8
Li Ziliang, Wen Ping. 2017. Comparison between the response of the Northwest Pacific Ocean and the South China Sea to Typhoon Megi (2010). Advances in Atmospheric Sciences, 34(1): 79–87, doi: 10.1007/s00376-016-6027-9
Lian Zhan, Fang Guohong, Wei Zexun, et al. 2015. A comparison of wind stress datasets for the South China Sea. Ocean Dynamics, 65(5): 721–734, doi: 10.1007/s10236-015-0832-z
Liu Junliang, Cai Shuqun, Wang Shengan. 2014. Diurnal wind and nonlinear interaction between inertial and tidal currents in the South China Sea during the passage of Typhoon Conson. Acta Oceanologica Sinica, 33(5): 1–7, doi: 10.1007/s13131-014-0467-9
Milliff R F, Large W G, Morzel J, et al. 1999. Ocean general circulation model sensitivity to forcing from scatterometer winds. Journal of Geophysical Research: Oceans, 104(C5): 11337–11358, doi: 10.1029/1998JC900045
Pan Jiayi, Sun Yujuan. 2013. Estimate of ocean mixed layer deepening after a typhoon passage over the South China Sea by using satellite data. Journal of Physical Oceanography, 43(3): 498–506, doi: 10.1175/JPO-D-12-01.1
Plueddemann A J, Farrar J T. 2006. Observations and models of the energy flux from the wind to mixed-layer inertial currents. Deep Sea Research Part II: Topical Studies in Oceanography, 53(1–2): 5–30
Pollard R T, Millard R C Jr. 1970. Comparison between observed and simulated wind-generated inertial oscillations. Deep Sea Research and Oceanographic Abstracts, 17(4): 813–821, doi: 10.1016/0011-7471(70)90043-4
Qu Tangdong. 2000. Upper-layer circulation in the South China Sea. Journal of Physical Oceanography, 30(6): 1450–1460, doi: 10.1175/1520-0485(2000)030<1450:ULCITS>2.0.CO;2
Rimac A, Von Storch J S, Eden C, et al. 2013. The influence of high-resolution wind stress field on the power input to near-inertial motions in the ocean. Geophysical Research Letters, 40(18): 4882–4886, doi: 10.1002/grl.50929
Silverthorne K E, Toole J M. 2009. Seasonal kinetic energy variability of near-inertial motions. Journal of Physical Oceanography, 39(4): 1035–1049, doi: 10.1175/2008JPO3920.1
Sprintall J, Roemmich D. 1999. Characterizing the structure of the surface layer in the Pacific Ocean. Journal of Geophysical Research: Oceans, 1042(C10): 23297–23311
Sprintall J, Tomczak M. 1992. Evidence of the barrier layer in the surface layer of the tropics. Journal of Geophysical Research: Oceans, 97(C5): 7305–7316, doi: 10.1029/92JC00407
Sun Chengxue, Liu Qinyu, Jia Yinglai. 2007. Annual and interannual variations of the mixed layer in the South China Sea. Periodical of Ocean University of China (in Chinese), 37(2): 197–203
Sun Lu, Zheng Quanan, Wang Dongxiao, et al. 2011. A case study of near-inertial oscillation in the South China Sea using mooring observations and satellite altimeter data. Journal of Oceanography, 67(6): 677–687, doi: 10.1007/s10872-011-0081-9
Tian Jiwei, Yang Qingxuan, Zhao Wei. 2009. Enhanced diapycnal mixing in the South China Sea. Journal of Physical Oceanography, 39(12): 3191–3203, doi: 10.1175/2009JPO3899.1
Von Storch J S, Sasaki H, Marotzke J. 2007. Wind-generated power input to the deep ocean: an estimate using a 1/10° general circulation model. Journal of Physical Oceanography, 37(3): 657–672, doi: 10.1175/JPO3001.1
Watanabe M, Hibiya T. 2002. Global estimates of the wind-induced energy flux to inertial motions in the surface mixed layer. Geophysical Research Letters, 29(8): 1239
Wu Qiaoyan, Chen Dake. 2012. Typhoon-induced variability of the oceanic surface mixed layer observed by Argo floats in the Western North Pacific Ocean. Atmosphere-Ocean, 50(S1): 4–14
Yang Qingxuan, Zhao Wei, Liang Xinfeng, et al. 2016. Three-dimensional distribution of turbulent mixing in the South China Sea. Journal of Physical Oceanography, 46(3): 769–788, doi: 10.1175/JPO-D-14-0220.1
Yang Qingxuan, Zhou Lei, Tian Jiwei, et al. 2015. The roles of Kuroshio intrusion and mesoscale eddy in upper mixing in the Northern South China Sea. Journal of Coastal Research, 30(1): 192–198
Zhai Xiaoming, Greatbatch R J, Eden C, et al. 2009. On the loss of wind-induced near-inertial energy to turbulent mixing in the upper ocean. Journal of Physical Oceanography, 39(11): 3040–3045, doi: 10.1175/2009JPO4259.1